Electronic Supplementary Information

Integrating photonic bandgap with surface plasmon resonance for enhancement of visible-light photocatalytic performance

Sugang Meng,[a,b] Danzhen Li,*[b] Xianliang Fu,[a] and Xianzhi Fu[b]

[a] Department of Chemistry, Huaibei Normal University, Anhui Huaibei, 235000, People's Republic of China.

[b] Research Institute of Photocatalysis, State Key Laboratory Breeding Base of Photocatalysis, Fuzhou University, Fuzhou, 350002, People's Republic of China.
Corresponding author Tel & Fax: (+86)591-83779256; E-mail: dzli@fzu.edu.cn

Experimental section

Materials. Styrene (≥ 99.0%), potassium persulfate (≥ 99.5%), methacrylic acid (≥ 98.0%), sulfuric acid (95.0-98.0%), hydrogen peroxide (≥ 30%), ethyl alcohol (≥ 99.7%), zinc nitrate hexahydrate (≥ 99.0%), sodium hydroxide (≥ 96.0%), rhodamine B (≥ 95%), p-chlorophenol (99.0%), zinc oxide (≥ 99.0%), sodium sulfate (≥ 99.0%), benzoquinone (≥ 98.0%), tert-butyl alcohol (≥ 99.0%), methyl alcohol (≥ 99.5%) and ammonium oxalate (≥ 99.5%) were all obtained from Sinopharm Chemical Reagent Co., Ltd. (Shanghai, China). 5, 5-dimethyl-1-pyrroline-N-oxide (≥ 95%) was obtained from Sigma Co..

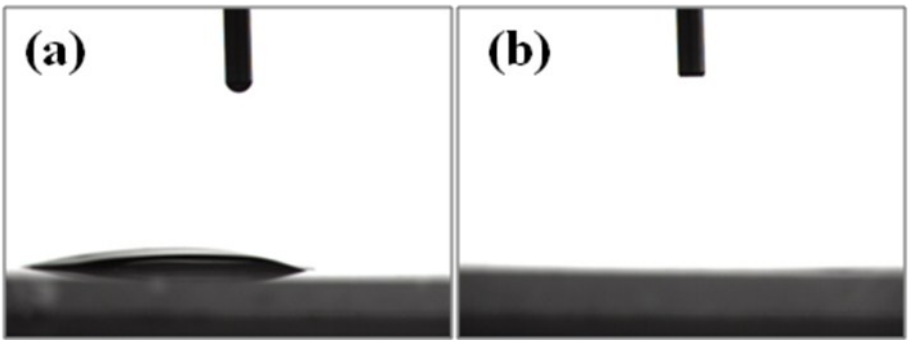

Fig. S1. Photographs of a water droplet on the slide surface: (a) the original slide, (b) the glass slide treated by H_2SO_4/H_2O_2 solution.

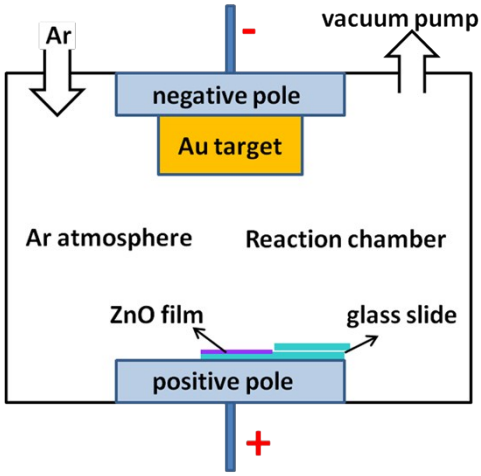

Scheme S1. Illustration of the magnetron sputtering.

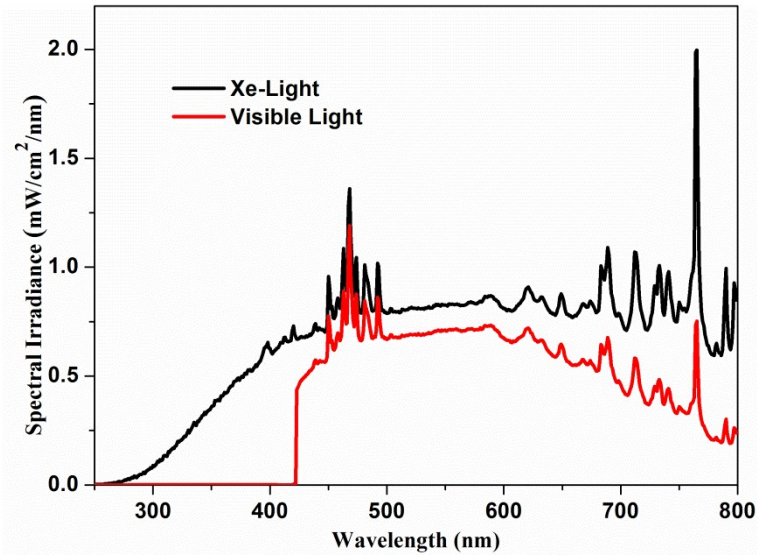

Fig. S2. The Spectral intensities emitted by a Xe-light source (visible light was obtained by the Xe-light source equipped with an IR-cutoff filter and an UV-cutoff filter).

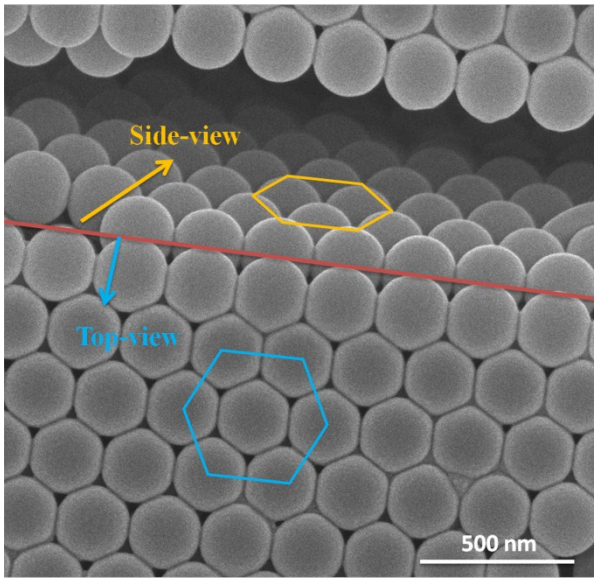

Fig. S3. A typical SEM image (Top-view and Side-view) of the PS opal template.

The side-view of the PS opal template has been detected by SEM. As shown in Fig. S3, the hexagonally close-packed PS spheres can be observed in both top-view and side-view.

Table S1. The amount of Au of Au/ZnO samples (Au wt.%).

Sample	Au/ZnO-P	Au/ZnO-182	Au/ZnO-222	Au/ZnO-277
Au wt.%	1.31	1.33	1.34	1.32

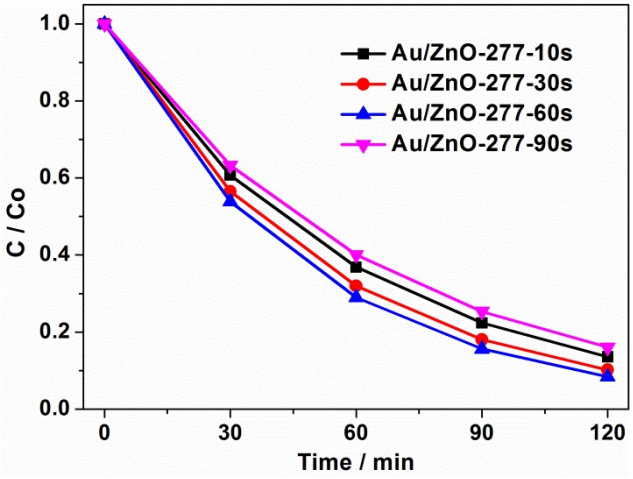

Fig. S4. The photocatalytic activity of Au/ZnO-277 coated with different amount of Au NPs for RhB degradation under visible light irradiation (Au/ZnO-277-60s is the Au/ZnO-277 mentioned in the manuscript, 10 s, 30 s, 60 s, and 90 s means the sputtering time).

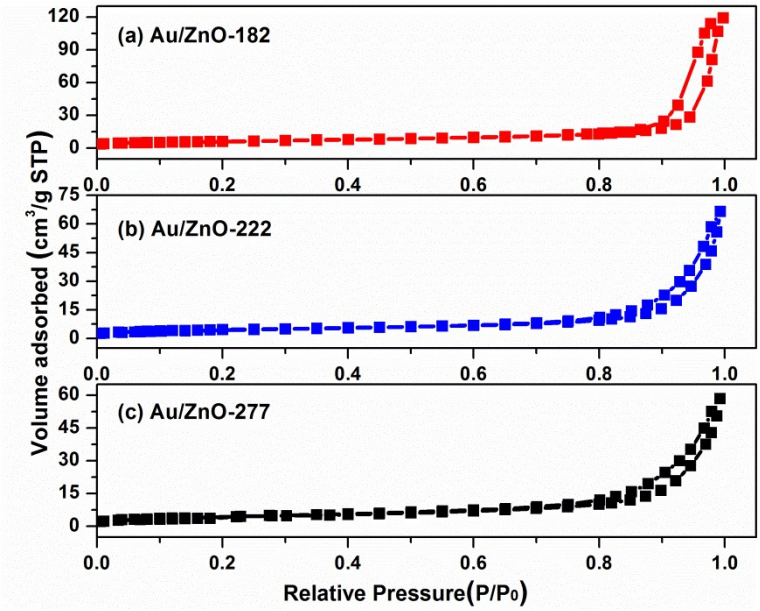

Fig. S5. Nitrogen adsorption-desorption isotherms of (a) Au/ZnO-182, (b) Au/ZnO-222 and (c) Au/ZnO-277.

The BET surface areas of Au/ZnO-182, Au/ZnO-222 and Au/ZnO-277 have been detected using a Micromeritics ASAP 2020 adsorption apparatus as suggested. The nitrogen adsorption-desorption isotherms of the samples are shown in Fig. S5 and the corresponding BET surface area is 21.2, 16.3 and 13.1 cm^2/g. It is clear that the surface areas of Au/ZnO-PCs decrease with the pore size, implying that the activity difference of Au/ZnO-PCs (decreases in order Au/ZnO-277 > Au/ZnO-222 > Au/ZnO-182) is not caused by the surface areas, but the photonic and SPR effects.

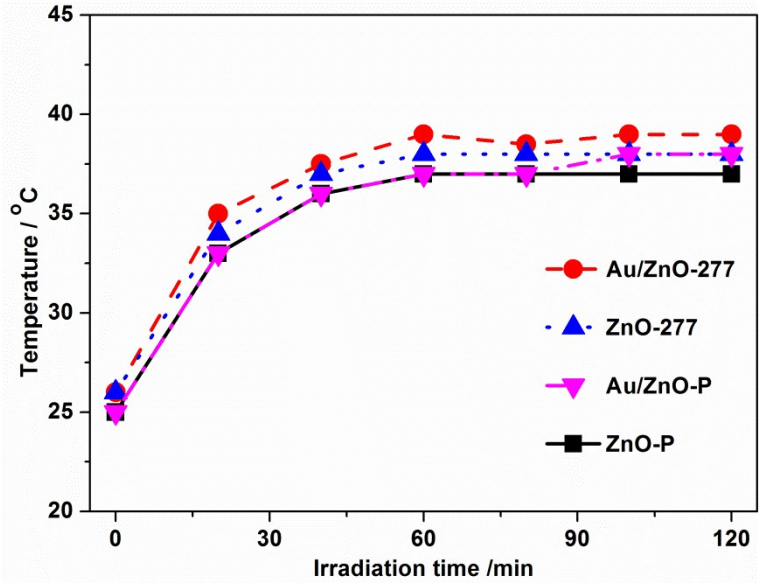

Fig. S6. The temperature profile during the photocatalytic measurements over ZnO-P, Au/ZnO-P, ZnO-277 and Au/ZnO-277.

In fact the reaction temperature has been controlled by an air conditioner (set at 25 ^{o}C) and a fan operated face to the reactor. To address this comment, the reactor temperatures during the photocatalytic measurements have been detected deliberately using ZnO-P, Au/ZnO-P, ZnO-277 and Au/ZnO-277 as representatives and the results are shown in Fig. S6. Apparently, as pointed in this comment, Au deposited ZnO-277 and ZnO-P showed a slight higher temperature (no more than 2 ^{o}C) than the pristine samples. However, we believe that this temperature difference is not large enough to alter the samples activity.

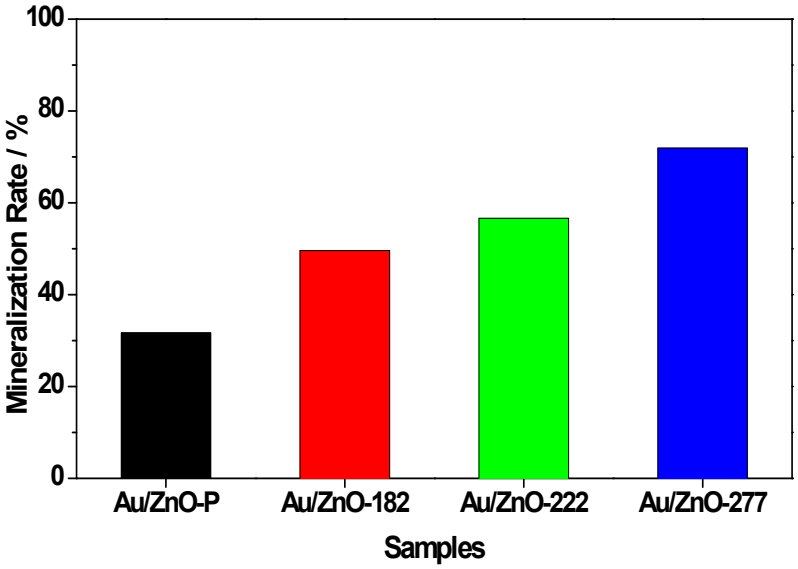

Fig. S7. The mineralization rate of RhB by different photocatalysts under visible light irradiation for 2 h.

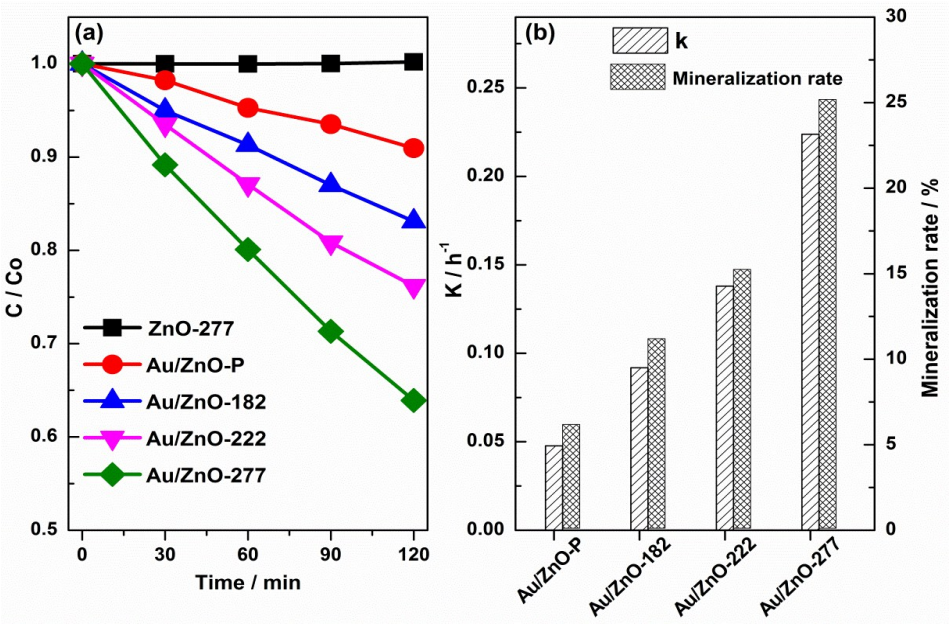

Fig. S8. (a) 4-chlorphenol degradation profile and (b) the kinetic constants (k) and mineralization rate over the as-prepared samples under visible light irradiation for 2 h.